Author Manuscript

Author Manuscript

Author Manuscript

Author Manuscript

HHS Public Access

Author manuscript

Biomacromolecules. Author manuscript; available in PMC 2021 October 12.

Published in final edited form as:

Biomacromolecules. 2020 October 12; 21(10): 4008–4016. doi:10.1021/acs.biomac.0c00580.

Polyamidoamine Dendrimer Grafted with an Acid-Responsive Charge-Reversal Layer for Improved Gene Delivery

Juan Wang[1,2,†], **Remy C. Cooper**[3,†], **Hu Yang**[2,4,5,*]

[1]College of Materials Science and Engineering, Sichuan University, Chengdu, Sichuan 610065, China

[2]Department of Chemical and Life Science Engineering, Virginia Commonwealth University, Richmond, Virginia 23219, United States

[3]Department of Biomedical Engineering, Virginia Commonwealth University, Richmond, Virginia 23284, United States

[4]Department of Pharmaceutics, Virginia Commonwealth University, Richmond, Virginia 23298, United States

[5]Massey Cancer Center, Virginia Commonwealth University, Richmond, Virginia 23298, United States

Abstract

We report on a heterogeneous dendrimer (G3-*acetal*-NH_2) derivative possessing an acid-responsive charge-reversal layer. The synthesis of G3-*acetal*-NH_2 starts with a polyamidoamine (PAMAM) G3 core and follows the aza-Michael addition with N-(2-(1-(allyloxy)ethoxy)ethyl)acrylamide (AEEAA) synthesized by us and the thiol-ene click chemistry with cysteamine hydrochloride in sequence. The surface of this newly formed dendrimer can turn from amine-terminated to hydroxyl-terminated due to the cleavage of the acetal groups in a weakly acidic environment. This charge conversion from 34.3 ± 2.7 mV to 18.0 ± 0.3 mV in 24 h at pH 5.3 enables its capacity as a therapy delivery vehicle. G3-*acetal*-NH_2 with a positively charged surface can condense pMAX GFP plasmid at similar weight ratios as native G4-NH_2 (above 2:1), allowing for its protected uptake into cells and endosomal escape. While in the endosome, the drop in vesicle pH cleaves the acetal bond, releasing the genetic payload and limiting its recondensation by the reduction in the dendrimer surface charge. When the vector/plasmid weight ratio was 2:1, G3-*acetal*-NH_2 improved transfection of pMAX GFP plasmid by 5-fold over native G4-NH_2 in NIH3T3 cells in terms of GFP protein expression. Taken together, we show that this surface charge conversion performance makes the synthesized heterogeneous dendrimer an improved vehicle for gene transfection.

*To whom correspondence should be addressed: hyang2@vcu.edu.

†J.W. and R.C.C. contributed equally to this work.

Supporting Information

Gel retardation assay of G4-NH2/pGFP (Fig. S1); gel retardation assay of G4-NH2/pGFP and G3-acetal-NH2/pGFP at 2:1weight ratios incubated for 0 h, 6 h, or 24 h in buffers at pH 7.4, pH 6.5, or pH 5.3 and NIH3T3 (Fig. S2); cells transfected with G3-acetal-NH2/gap (Fig. S3).

The authors declare no competing financial interest.

Author Manuscript
Author Manuscript
Author Manuscript
Author Manuscript

Graphical Abstract

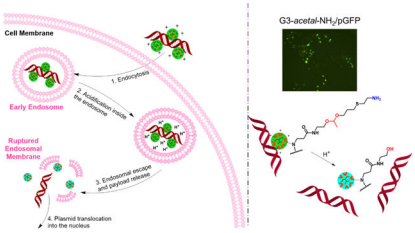

Keywords

dendrimer; acid-labile; cleavable; charge-transfer; gene transfection

INTRODUCTION

Gene therapy has become a therapeutic option for many diseases including cancer treatment.[1–3] Challenges to attaining the effectiveness of gene therapy persist: (1) the trade-off of transfection efficiency and safety when choosing between viral and non-viral vectors;[4, 5] (2) the effect's duration for the type of DNA integration or residence of siRNA in the cytoplasm;[6] (3) the delivery of nucleic acids to the target site.[7] A gene delivery system ideally has the features of both low toxicity and high transfection efficiency.[8] Polyamidoamine (PAMAM) dendrimers with primary amine termini have been extensively explored as non-viral gene carriers.[9–13] The highly cationic charges on the dendrimer surface can facilitate its complexation with the negatively charged phosphate-backbone of nucleic acids. However, nucleic acid/PAMAM complexes are thermodynamically stable and inherently resistant to dissociation, restricting the release of the nucleic acid from the carrier.[7, 14] To improve gene transfection, one must promote the separation of nucleic acid from carriers following cellular internalization and endosomal escape.[14] It is vital to design a responsive gene carrier that can release nucleic acids, such as thermo-, photo- and pH-sensitive delivery systems, as well as osmotic pressure and biological signal responsive systems.[15, 16] Recent literature has reported charge-reversal gene vectors with the ability to respond to intracellular signals to release packed nucleic acid and thus gain enhanced gene transfection efficiency.[17–20]

Herein, we synthesized a heterogeneous dendrimer (G3-*acetal*-NH_2) with an acid-responsive charge-reversal layer starting with a PAMAM G3 core following a two-step click reaction. We tested whether the surface of this newly formed dendrimer could turn from amine-terminated to hydroxyl-terminated as a result of the cleavage of acetal bonds in a weakly acidic environment and assessed G3-*acetal*-NH_2 for its ability to deliver genes and transfect cells. Our results show that grafting low generation dendrimer with an acid-responsive charge-reversal layer holds the potential to improve gene transfection.

Author Manuscript Author Manuscript Author Manuscript Author Manuscript

Materials and Methods

Materials.

EDA-core amine-terminated PAMAM dendrimer generations 3 and 4 (G3-NH_2, G4-NH_2) and hydroxyl-terminated PAMAM dendrimer generation G4 (G4-OH) were purchased from Dendritech (Midland, MI). *N*-(2-hydroxyethyl) acrylamide, pyridinium *p*-toluenesulfonate (PPTS, ≥ 99.0%), 2-dimethoxy-2-phenylacetophenone (DMPA, 99%), potassium carbonate (K_2CO_3, ≥ 99.0%) were purchase from Sigma-Aldrich (St. Louis, MO). Allyl vinyl ether (95%) was purchased from Alfa Aesar (Tewksbury, MA). Cysteamine hydrochloride was purchased from Chem-Impex International, Inc (Wood Dale, IL). Potassium dihydrophosphate (KH_2PO_4) and disodium hydrogen phosphate (Na_2HPO_4) were purchased from Fisher. Cosmic calf serum and pMAX-GFP (pGFP) plasmid were purchased from Lonza (Walkersville, MD). Ethidium bromide, Dulbecco's modified Eagle medium (DMEM), trypsin-EDTA (0.25%), and penicillin-streptomycin (10,000 U/mL) were purchased from Life Technologies (Carlsbad, CA). Cell proliferation reagent WST-1, PhosSTOP™ and cOmplete™ ULTRA Protease Inhibitor Cocktail Tablets were purchased from Roche Applied Science (Indianapolis, IN).

Synthesis of *N*-(2-(1-(allyloxy)ethoxy)ethyl)acrylamide (AEEAA).

The monomer AEEAA was synthesized following the reported procedure.[19] *N*-(2-hydroxyethyl) acrylamide (12 mmol) and PPTS (1 mmol) were dissolved in 10 mL of anhydrous DCM and stirred at 0 °C for 30 min. Allyl vinyl ether (10 mmol) in 5 mL of anhydrous DCM was added dropwise to the mixture. The reaction was stirred at room temperature overnight, and then excess K_2CO_3 was added to quench the reaction. The mixture was filtered, and the filtrate was concentrated under reduced pressure to obtain a crude product. The product was further purified by using flash chromatography (hexane/ethyl acetate (v/v=1/1) as eluent) to obtain AEEAA as a liquid product. The product yield was 75%. ^{1}H NMR (600 MHz, $CDCl_3$, ppm): δ 6.27 (dd, *J* = 17.0, 1.4 Hz, 1H), 6.11 (d, *J* = 10.3 Hz, 1H), 5.89 (ddt, *J* = 17.0, 10.5, 5.6 Hz, 1H), 5.63 (dd, *J* = 10.3, 1.4 Hz, 1H), 5.35–5.25 (m, 1H), 5.19–5.12 (m, 1H), 4.73 (d, *J* = 5.3 Hz, 1H), 4.12–3.95 (m, 2H), 3.70–3.48 (m, 4H), 1.32 (d, *J* = 5.3 Hz, 3H). ^{13}C NMR (600 MHz, $CDCl_3$, ppm): δ 165.73, 134.71, 130.95, 126.72, 117.29, 99.89, 67.23, 64.24, 39.99, 20.04.

Synthesis of G3-*acetal*-ene.

G3-NH_2 (15 μmol) and AEEAA (538 mg, 2.7 mmol) were mixed in 2 mL of methanol/water (v/v:7/3) and stirred at 70 °C for 48 h. The mixtures were then dialyzed in deionized water using SnakeSkin dialysis tubing (MWCO 1 kDa) and freeze-dried to obtain G3-*acetal*-ene. The yield was 80%. ^{1}H NMR (600 MHz, MeOD, ppm): δ 5.98–5.86 (m, 43 H), 5.28 (d, *J* = 11.5 Hz, 44 H), 5.14 (d, *J* = 6.9 Hz, 44 H), 4.75 (dq, *J* = 7.0, 3.5 Hz, 49 H), 4.15–4.01 (m, 90 H), 3.71–3.59 (m, 106 H), 3.54 (dddd, *J* = 12.4, 10.1, 5.4, 3.1 Hz, 68 H), 3.47–3.41 (m, 54 H), 3.37 (d, *J* = 3.8 Hz, 78 H), 3.27 (d, *J* = 3.8 Hz, 92 H), 2.80 (d, *J* = 4.3 Hz, 184 H), 2.59 (d, *J* = 4.0 Hz, 92 H), 2.37 (s, 184 H), 1.29 (dd, *J* = 3.6, 1.2 Hz, 150 H).

Author Manuscript Author Manuscript Author Manuscript Author Manuscript

Synthesis of G3-*acetal*-NH_2.

G3-*acetal*-ene (3 μmol), DMPA (2 μmol), and cysteamine hydrochloride (420 μmol) were mixed in 2 mL of methanol. The reaction mixture was irradiated under a 365 nm UV lamp at room temperature for 4 h, dialyzed in deionized water using SnakeSkin dialysis tubing (MWCO 1 kDa) and freeze-dried to obtain G3-*acetal*-NH_2. The yield was 70%. ^{1}H NMR (600 MHz, D_2O, ppm): δ 4.73 (m, 42 H), 3.72–3.59 (m, 98 H), 3.58–3.47 (m, 130 H), 3.37–3.16 (m, 280 H), 3.09 (dd, J = 30.1, 23.2 Hz, 98 H), 2.73 (d, J = 6.1 Hz, 330 H), 2.56 (dd, J = 8.8, 5.7 Hz, 244 H), 2.42–2.27 (m, 244 H), 1.77 (dd, J = 12.6, 6.3 Hz, 74 H), 1.22 (d, J = 5.2 Hz, 150 H). ^{13}C NMR (600 MHz, D_2O, ppm): δ 174.16, 100.59, 64.76, 64.15, 59.91, 49.20, 41.51, 39.31, 38.30, 28.66, 28.19, 27.37, 19.14.

Characterization.

Nuclear Magnetic Resonance (NMR) Spectroscopy.—^{1}H NMR and ^{13}C NMR spectra of dendrimer derivatives were obtained on a Bruker 600 MHz spectrometer.

High Performance Liquid Chromatography (HPLC).—Dendrimer derivatives were characterized by using an HPLC (Waters) system equipped with a Waters 1515 isocratic HPLC pump, a Waters 2487 dual λ absorbance detector and a Waters 717 plus autosampler. The mobile phase was a mixture of acetonitrile/water (v/v = 1/1). The eluents were monitored by the UV detector at 220 nm and 360 nm.

Zeta Potential and Size Measurements.—The zeta potentials and hydrodynamic sizes of dendrimer derivatives, as well as the sizes of dendrimer/pGFP complexes, were determined by using Malvern Zetasizer Nano ZS90 (Malvern Instruments, Worcestershire, U.K.).

Test of acid-responsiveness of G3-*acetal*-NH_2.

Deuterated phosphate buffer (pH 5.3) was prepared by mixing 9.5 mL of potassium dihydrophosphate solution (0.067 M) with 0.5 mL of disodium hydrogen phosphate solution (0.067 M). Both the potassium dihydrophosphate solution and disodium hydrogen phosphate solution were prepared using deuterated oxide (D_2O) as the solvent. G3-*acetal*-NH_2 was directly dissolved in deuterated phosphate buffer at pH 5.3. Following 24 h-incubation at 37 °C, ^{1}H NMR spectra of G3-*acetal*-NH_2 were recorded. The cleavage of acetal bonds was calculated based on the reduction of the integration of the peaks at 1.31 ppm (methyl in the acetal groups).

Cytotoxicity of G3-*acetal*-NH_2.

Two cell lines, including NIH3T3 mouse embryo fibroblast cells and HN12 head and neck cancer squamous cell carcinomas, were used to test the cytotoxicity of G3-*acetal*-NH_2. Cells were seeded in a 96-well plate at a density of 1×10^4 cells/well. After 24 h, the culture medium was replaced with 200 μL of fresh medium containing G3-*acetal*-NH_2 at different concentrations (0.2, 2, 20, 100, 200 μg/mL, n = 6). Cell viability after 24 h incubation was determined by using WST-1 assay.

Author Manuscript Author Manuscript Author Manuscript Author Manuscript

pGFP binding and acid-responsive destabilization gel retardation assays.

G4-OH was mixed with pMAX GFP plasmid at weight ratio of 5:1 and 10:1. The mixtures were vortexed for 10 s and left to equilibrate at room temperature for a minimum of 30 min. Similarly, native G4-NH_2 and G3-*acetal*-NH_2 was complexed with pMAX GFP plasmid at weight ratios of 1:1, 2:1, and 4:1. The prepared complexes were subjected to gel retardation assay as described in our previous work.[21]

G4-NH_2 and G3-*acetal*-NH_2 complexed with pGFP at weight ratios of 2:1 were prepared as previously described and incubated at 37 °C for 0, 6 and 24 h in pH 7.4, 6.5 and 5.3 buffer. The 0 h samples were immediately loaded into 1% agarose gels after complexation without 37 °C incubation. All gels were ethidium bromide stained, run at 100 V for 30 minutes and visualized using a UV transilluminator. Band intensities were quantified using ImageJ software.

Transfection evaluation.

NIH3T3 cells were seeded in 12 well plates at a density of 3×10^4 cells/well and allowed to attach overnight. G4-NH_2/pGFP and G3-*acetal*-NH_2/pGFP polyplexes at weight ratio of 2:1 were added to the cell culture medium and incubated for 6 h at 37 °C followed by fresh media change and further incubation for 72 h. Fluorescence microcopy was performed on a Nikon Eclipse Ti-U inverted fluorescence microscope (Melville, NY) using FITC channel and brightfield. Each group was repeated in triplicate and GFP-expressing cells counted using ImageJ software.[22] Another set of cells prepared and treated as described above were lysed with cell lysis buffer containing phosphatase and protease inhibitors for protein extraction to measure the GFP fluorescence signal on a Nanodrop 3300 fluorospectrometer (Waltham, MA).

Statistical analysis.

All data is expressed as means ± standard deviations (SD) and tested with a one-way analysis of variance (ANOVA), with differences between groups assessed via Tukey-HSD. A p-value of < 0.05 was considered statistically significant.

RESULTS AND DISCUSSION

Characterization of G3-acetal-NH_2.

First, an acetal monomer *N*-(2-(1-(allyloxy)ethoxy)ethyl)acrylamide (AEEAA) was synthesized by a click-type reaction of hydroxyl and vinyl ether in the presence of PPTS (Scheme 1A). The structure of AEEAA was verified with its ^{1}H NMR and ^{13}C NMR spectra (Fig. 1). The peaks at 4.73 ppm and 1.32 ppm in ^{1}H NMR (Fig. 1A) and 99.89 ppm and 20.04 ppm in ^{13}C NMR (Fig. 1B) were attributed to the acetal group, indicating the successful synthesis of AEEAA.

The acid-labile dendrimer of G3-*acetal*-NH_2 was obtained *via* a two-step synthesis (*aza*-Michael addition and thiol-ene click chemistry) using PAMAM G3-NH_2 as the core (Scheme 1B). The chemical structures of G3-*acetal*-ene and G3-*acetal*-NH_2 were well verified by their ^{1}H NMR spectra (Fig. 2) compared to that of PAMAM G3 (Fig. 2). The

Author Manuscript Author Manuscript Author Manuscript Author Manuscript

peaks at 5–6 ppm attributed to the alkenes in G3-*acetal*-ene proved the success of the *aza*-Michael addition. Based on the integral ratio of acetal groups at 1.29 ppm to PAMAM G3 protons at 2.37, 2.59, 2.80, 3.27, 3.37, and 3.43 ppm, there were 50 AEEAAs on average conjugated to G3. The alkenes in G3-*acetal*-ene disappeared completely in the spectra of G3-*acetal*-NH_2, and the peaks at 1.77 ppm attributed to the newly formed methylene appeared, indicating that all the alkene groups were successfully reacted with cysteamine (Fig. 2). The disappearance of alkenes in G3-*acetal*-ene is also confirmed by ^{13}C NMR spectrum shown in Fig. 2B. Given the number of AEEAA molecules reacted onto the G3 surface and the subsequent reaction to produce amine termini, G3-(*acetal*-NH_2)$_{50}$ is comparable to a native G4-NH_2 dendrimer with 64 surface amines. For all subsequent assays, this formulation will be compared with G4-NH_2.

High-performance liquid chromatography characterization conducted on G3, G3-*acetal*-ene, and G3-*acetal*-NH_2 (Fig. 3) confirmed their purity. As G3-NH_2 was converted to G3-*acetal*-NH_2, the molecular weight of G3-*acetal*-NH_2 increased, and its polarity decreased. Compared to G3-NH_2, the eluent time of G3-*acetal*-ene and G3-*acetal*-NH_2 shifted to 1.70 min and 2.03 min.

The ζ potentials of G3-NH_2 and G4-NH_2 are 5.2 ± 0.6 mV and 27.7 ± 1.4 mV, respectively (Fig. 4A). Since the surface of G3-*acetal*-ene is composed of mostly -ene groups, the ζ potential of G3-*acetal*-ene is slightly negative, i.e., −1.6 ± 0.4 mV. G3-*acetal*-NH_2 is amine-terminated, and its ζ potential is 34.3 ± 2.7 mV, which is comparable with that of G4-NH_2. We measured the size of the dendrimer and plasmid components, as well as complexes (at 2:1 weight ratio used in transfection). G3-*acetal*-NH_2 shows a slightly larger hydrodynamic size (9.9 ± 1.8 nm) compared with G3-NH_2 (5.4 ± 0.8 nm) and G4-NH_2 (5.6 ± 0.6 nm). The increased size of G3-*acetal*-NH_2 compared with G4-NH_2 might because of a longer and more hydrophilic peripheral molecular chains. All dendrimer/plasmid complexes (at 2:1 weight ratio used in transfection) are nanosized, which are small enough for cellular uptake.

Charge-transfer behavior.

After culturing the acid-labile dendrimer of G3-*acetal*-NH_2 in pH 5.3 for 24 h and 48 h, the ζ potential changed to be 18.0 ± 0.3 mV and 16.3 ± 0.5 mV, respectively (Fig. 5B). This sharp decline on ζ potential indicates that a large proportion of the terminated groups on the dendrimer surface have turned from -NH_2 to -OH by the cleavage of the acetal groups (Fig. 5A). As shown in Fig. 6,^1H NMR spectrum of G3-*acetal*-NH_2 after culturing at pH 5.3 for 24 h shows the reduction of acetal groups at 1.32 ppm and the appearance of aldehyde groups (-C*H*O, 9.75 ppm) on acetaldehyde. Calculated by the reduction of the integration ratio of a/b, there is approximately 17% of terminated groups changed from -NH_2 to -OH after 24 h culturing at pH 5.3. The decrease of ζ potential as well as the changes seen in ^1H NMR spectrum confirmed the charge-reversal capacity of G3-*acetal*-NH_2 at pH 5.3. The reason for not 100% charge-reversal is assumed to be the steric hindrance of the chains and inability of the H^+ ions to penetrate to all chains in the dendrimer.[19]

Author Manuscript Author Manuscript Author Manuscript Author Manuscript

Cytotoxicity.

Cytotoxicity study revealed that G3-*acetal*-NH_2 is highly cytocompatible both on NIH3T3 cells and HN12 cells. It did not cause toxicity up to 200 μg/mL following 24 h exposure on NIH3T3 cells (Fig. 7A). When the concentration is 100 μg/mL and 200 μg/mL, a reduction of less than 25% and 40% viability was observed in HN12 cells (Fig. 7B). This drop in cell viability at the higher concentration ranges is due to the anticipated variances in cell responses to different treatments. However, the trend in biocompatibility across a useful concentration of G3-*acetal*-NH_2 is similar between the two cell types, indicating that no toxicity is expected from the formulation within the 0.2 – 100 μg/mL concentration range.

Gene complexation and acid-responsive destabilization evaluation.

To examine whether this acid-labile dendrimer G3-*acetal*-NH_2 can be used as efficient gene transfection carriers, we tested the DNA binding of both G4-OH and G3-*acetal*-NH_2. Fig. 8A shows that −OH terminated G4 dendrimer (G4-OH) cannot bind with DNA. The lack of a cationic surface charge on the G4-OH prevents the plasmid DNA interaction, suggesting that products of G3-*acetal*-NH_2/plasmid after cleavage in weak acid will not re-associate. Native G4-NH_2/pGFP for neutral complexes above a 0.5:1 ratio (Fig. S1), while G3-*acetal*-NH_2/pGFP begins to form neutrally charged complexes at a 2:1 ratio between (Fig. 8B). Although there is some signal in the 2:1 lane for G3-*acetal*-NH_2, it appears to consist of the supercoiled plasmid DNA with signal remaining in the well. These results suggest that more G3-*acetal*-NH_2 is required to form stable complexes due to the slight reduction in available surface primary amines as a result of the acetal bond incorporation.

While the charge reversal and effective complexation of the modified dendrimer has been illustrated, we further tested the destabilization of the complex at relevant pH buffers to mimic the acidification of the intracellular environment after nanoparticle endocytosis (Fig. S2). As expected, G4-NH_2/pGFP complexes at a ratio of 2:1 do not undergo destabilization with a reduction in pH over 24 h since there are no hydrolyzable moieties in the native dendrimer structure. G4-NH_2 effectively protects the plasmid payload from degradation since no bands are seen in the gels (Fig. S2 A–C). However, the cleavable G3-*acetal*-NH_2 formulations show degradation across all time points and pH values. The 0 h and 6 h gels similarly suggest that there is a higher amount of degradation of signal in the lower pH samples relative to pH 7.4. This is evident, first, by observing the total intensity (T) values of the pGFP control wells relative to the G3-*ac*-NH_2/pGFP lanes: The pGFP lanes contain the total amount of plasmid since they are negatively charged and will only run between the wells (negative electrode end) and the positive electrode. The other lanes include the dendrimers at 2:1 weight ratio (constant plasmid amount) that would affect the direction of the plasmid signal movement. For the pH 7.4 G3-*ac*-NH_2/pGFP lanes, the total signal intensities are 17213 a.u. and 13599 a.u. in the 0 h and 6 h gels, respectively (Fig. S2 A, B). These values are lower than the pGFP control lane intensities (29573 $a.u._{0h}$/29752 $a.u._{0h}$ and 30469 $a.u._{6h}$/28815 $a.u._{6h}$), suggesting that some signal is absent either due to stable complexation with a positively charged surface that would cause them to move toward the negative electrode or some degradation due to the buffer pH. The former is more probable for these pH 7.4 lanes, since degradation of the plasmid is not expected at neutral pH. Likewise in the pH 6.5 and 5.3 lanes in the 0 h and 6 h gels, the total signal intensities are

Author Manuscript Author Manuscript Author Manuscript Author Manuscript

further reduced relative to control pGFP and pH 7.4 (12856 a.u.$_{0h,pH\ 6.5}$; 10683 a.u.$_{0h,pH\ 5.3}$; 8423 a.u.$_{6h,pH\ 6.5}$; 6183 a.u.$_{6h,pH\ 5.3}$). It is unlikely that the lower pH buffers would cause the complexes to carry a more positive surface charge. Therefore, the signal intensity reduction is driven primarily by the degradation of the released and unprotected plasmid. Another confirmation of increased release and plasmid degradation in the lower pH buffers is the observation of signal intensity in the wells, which represent neutrally charged complexes. Like with total lane intensity, higher well signal intensity (W) is seen in the pH 7.4 samples with gradual signal reduction corresponding to decreasing pH. This translates to more stable complexes being observed in the wells of complexes incubated at neutral pH. The 24 h gel does not exactly mimic the 0 h and 6 h gels in terms of band smearing patterns across the pH values, which we attribute to the overall degradation of the samples over the longer term exposure at 37 °C especially in the lower pH buffers (Fig. S2 C).

Gene transfection.

NIH3T3 cells were transfected with either G4-NH_2/pGFP or G3-*acetal*-NH_2/pGFP at a weight ratio of 2:1 so that stable complexes of both formulations would form, while preventing overly cationic polyplexes that could limit dissociation. Fluorescence microscopy using a FITC channel revealed effective transfection in the cleavable dendrimer formulation, but no visibly transfected cells in the native G4-NH_2/pGFP sample at this weight ratio (Fig. 9A). Cell counting resulted in 3780 GFP-expressing cells ± 847 out of a total of roughly 300,000 cells (Fig. S3) by the end of the incubation period based on initial seeding density of 30,000 cells/well. While this translates to a transfection efficiency of only 1.26%, it improves the transfection ability of native G4-NH_2 since no transfected cells were observed in those wells. This was further confirmed by measuring the fluorescence intensity of whole cell lysate extracted proteins containing GFP at an emission wavelength of 503 nm. Relative to untreated cells, proteins from the G4-NH_2/pGFP sample resulted in an RFU of 120.2 ± 46.0 while G3-*acetal*-NH_2/pGFP gave an RFU of 658.3 ± 175.3 (Fig. 9B). With one-way ANOVA test statistic of 33.7 and a p-value of 0.0005, the difference in green fluorescent proteins between the two treatment groups is significant.

We postulate that the lack of GFP-expressing cells in the microscopy images compared to the slight signal of extracted GFP from the fluorospectrometer is a result of the more sensitive detection of the latter approach. The improved transfection efficiency of the cleavable dendrimer relative to native G4-NH_2 is demonstrated, likely due to the ability of the acetal bond to be cleaved in the early endosome prior to and during endosomal escape. Colocalization of fluorescently labeled vehicle and plasmid would help elucidate at what stage of intracellular trafficking the acetal bond is cleaved, and dissociation of the dendrimer and plasmid components takes place. We have seen previously in confocal laser microscopy images (data not shown) that FITC-G4-NH_2 and Cy3-labeled plasmid are associated through cellular uptake, endosomal escape, and cytosolic accumulation, with very little signal dissociation or penetration into the nucleus. While this pH-labile functionalization is a likely cause of the increased transfecting ability, the surface zeta potential may also be contributing to the difference between native and modified dendrimer.

Author Manuscript Author Manuscript Author Manuscript Author Manuscript

As previously mentioned, the incorporation of the acetal bond functionality results in 50 total surface amines compared to 64 owned by a native G4-NH_2. This slight reduction in surface charge, and the associated increase in the required weight ratio for G3-*acetal*-NH_2/pGFP complex stabilization compared to G4-NH_2/pGFP also suggests that at the same ratio of 2:1 for both treatments, G3-*acetal*-NH_2/pGFP is less strongly associated than G4-NH_2/pGFP. This suggests a weaker interaction and easier dissociation. However, we expect the dendrimer/plasmid dissociation to be the rate-limiting step, and therefore the difference in surface charges to minimally contribute to the increased transfecting ability of the G3-*acetal*-NH_2 formulation.[23, 24]

It has been widely acknowledged that three main reasons account for low transfection of dendrimers: 1) low cell internalization; 2) early dissociation of plasmid in the early endosome; 3) low plasmid dissociation after the endosome escape. Since G3-*acetal*-NH_2 has a similar number of amine termini to G4-NH_2, and G4-NH_2 has been broadly demonstrated to have excellent cell internalization ability, we do not doubt the cell internalization capacity of G3-*acetal*-NH_2. We postulate that the limited transfection of G4-NH_2 is mainly due to its low plasmid dissociation after endosome escape. Based on our observation that G3-*acetal*-NH_2 has higher transfection efficiency than G4-NH_2, it is assumed that at least some of the acetal bonds were cleaved during endosomal retention and escape.

^{1}H NMR, zeta potential and gel mobility shift results indicate an incomplete charge reversal of G3-*acetal*-NH_2 from amine to hydroxyl at pH 5.3. This slow hydrolysis of the acetal bonds leads to a ‘fractured’ dendrimer in the endosome step. Tang et al reported a ‘fractured’ dendrimer enhanced gene transfection efficiency dramatically (>50-fold).[25] This modified PAMAM dendrimer is degradable under heat treatment, resulting in a hetero-dispersed population of compounds with molecular weights ranging from very low (<1,500 Da) to several tens of kilodaltons. The defective branching was found improved transfection activity compared to that of the intact dendrimers. In addition, based on literature reports, both surface charges and hydrophobicity of PAMAM affect its complexation with plasmid, a decrease of electrostatic interactions and more hydrophobic packing of DNA in PAMAM dendrimers can significantly reduce their capacity of gene association.[26, 27] Although we cannot reach 100% of charge reversal, the partial transition of amine to hydroxyl also increases the hydrophobicity of the dendrimer, which amplified the effect of charge conversion on plasmid dissociation.

This work demonstrates the functionality of the acetal-linker in reduced pH environments as would be found in trafficking compartments such as the early and late endosome, as well as the enhanced transfection ability of the cleavable dendrimer as a gene carrier. However, further work is necessary to understand the exact mechanism and temporal-spatial location of G3-*acetal*-NH_2 and hydrolysis of the acetal linkage to complement the gel mobility data of samples incubated in varying pH buffers over time. This can be explored by fluorescently tagging the modified dendrimer and a plasmid and observing the complexes using real-time confocal microscopy to determine where dissociation is occurring in the intracellular trafficking, as well as monitoring if plasmid signal can be found within the nucleus over time. Flow cytometry could also be employed to determine the difference in labeled-plasmid uptake between the G3-*acetal*-NH_2 and G4-NH_2 control and to ensure that the enhanced

Author Manuscript Author Manuscript Author Manuscript Author Manuscript

transfection efficiency derives from the acetal bond cleavage and not from the difference in the plasmid uptake. Additionally, given the hydrolysis of only ~17% of the available acetal-chains on the G3-*acetal*-NH_2 over 24 h at reduced pH, the grafting density could be optimized to reduce the number of the stimuli-responsive chains, allowing for further modification such as for enhanced biocompatibility or cell-specific targeting. This functionalization could also be utilized for the delivery of other therapeutics, such as surface-grafted drug molecules.

CONCLUSIONS

An acid-liable layer was grafted onto PAMAM dendrimer via acetal bonds to make a heterogeneous dendrimer. This newly formed dendrimer exhibits charge transfer property from positive charge to neutral in a weakly acidic environment. This charge conversion performance as well makes the synthesized heterogeneous dendrimer an improved vehicle for gene transfection.

Supplementary Material

Refer to Web version on PubMed Central for supplementary material.

ACKNOWLEDGMENTS

This work was supported, in part, by the National Institutes of Health (R01EY024072 and R01HL140684). Microscopy was performed at the Virginia Commonwealth University Microscopy Facility, supported, in part, by funding from NIH-NCI Cancer Center Support Grant P30CA016059.

REFERENCES

1. Wang YH; Su HH; Yang Y; Hu YX; Zhang L; Blancafort P; Huang L Systemic delivery of modified mRNA encoding herpes simplex virus 1 thymidine kinase for targeted cancer gene therapy. Mol. Ther 2013, 21 (2), 358–367. [PubMed: 23229091]
2. Chen ZM; Liu FY; Chen YK; Liu J; Wang XY; Chen AT; Deng G; Zhang HY; Hong ZY; Zhou JB Targeted delivery of CRISPR/Cas9-mediated cancer gene therapy via liposome-templated hydrogel nanoparticles. Adv. Funct. Mater 2017, 27 (46), 1703036. [PubMed: 29755309]
3. Ginn SL; Amaya AK; Alexander IE; Edelstein M; Abedi MR Gene therapy clinical trials worldwide to 2017: an update. J. Gene Med 2018, 20 (5), e3015. [PubMed: 29575374]
4. Teo PY; Yang C; Hedrick JL; Engler AC; Coady DJ; Ghaem-Maghami S; George AJT; Yang YY Hydrophobic modification of low molecular weight polyethylenimine for improved gene transfection. Biomaterials 2013, 34 (32), 7971–7979. [PubMed: 23880339]
5. Baruteau J; Waddington SN; Alexander IE; Gissen P Gene therapy for monogenic liver diseases: clinical successes, current challenges and future prospects. J. Inherited Metab. Dis 2017, 40 (4), 497–517. [PubMed: 28567541]
6. Stepanenko AA; Heng HH Transient and stable vector transfection: pitfalls, off-target effects, artifacts. Mutat. Res., Rev. Mutat. Res 2017, 773, 91–103.
7. Veron L; Ganee A; Ladaviere C; Delair T Hydrolyzable p(DMAPEMA) polymers for gene delivery. Macromol. Biosci 2006, 6 (7), 540–554. [PubMed: 16921541]
8. Jin L; Zeng X; Liu M; Deng Y; He NY Current progress in gene delivery technology based on chemical methods and nano-carriers. Theranostics 2014, 4 (3), 240–255. [PubMed: 24505233]
9. Yuan QA; Yeudall WA; Yang H PEGylated Polyamidoamine dendrimers with bis-aryl hydrazone linkages for enhanced gene delivery. Biomacromolecules 2010, 11 (8), 1940–1947. [PubMed: 20593893]

Author Manuscript Author Manuscript Author Manuscript Author Manuscript

10. Bae Y; Green ES; Kim GY; Song SJ; Mun JY; Lee S; Park JI; Park JS; Ko KS; Han J; Choi JS Dipeptide-functionalized polyamidoamine dendrimer-mediated apoptin gene delivery facilitates apoptosis of human primary glioma cells. Int. J. Pharm 2016, 515 (1–2), 186–200. [PubMed: 27732896]
11. Vaidyanathan S; Chen J; Orr BG; Holl MMB Cationic polymer intercalation into the lipid membrane enables intact polyplex DNA escape from endosomes for gene delivery. Mol. Pharmaceutics 2016, 13 (6), 1967–1978.
12. Xu LY; Kittrell S; Yeudall WA; Yang H Folic acid-decorated polyamidoamine dendrimer mediates selective uptake and high expression of genes in head and neck cancer cells. Nanomedicine *(London, U. K.)* 2016, 11 (22), 2959–2973. [PubMed: 27781559]
13. Li J; Liang HM; Liu J; Wang ZY Poly (amidoamine) (PAMAM) dendrimer mediated delivery of drug and pDNA/siRNA for cancer therapy. Int. J. Pharm 2018, 546 (1–2), 215–225. [PubMed: 29787895]
14. Sonawane ND; Szoka FC; Verkman AS Chloride accumulation and swelling in endosomes enhances DNA transfer by polyamine-DNA polyplexes. J. Biol. Chem 2003, 278 (45), 44826–44831. [PubMed: 12944394]
15. Qiu NS; Liu XR; Zhong Y; Zhou ZX; Piao Y; Miao L; Zhang QZ; Tang JB; Huang L; Shen YQ Esterase-activated charge-reversal polymer for fibroblast-exempt cancer gene therapy. Adv. Mater 2016, 28 (48), 10613–10622. [PubMed: 27786373]
16. Kim J; Kim H; Kim WJ, Single-Layered MoS2-PEI-PEG Nanocomposite-Mediated Gene Delivery Controlled by Photo and Redox Stimuli. Small 2016, 12 (9), 1184–1192. [PubMed: 26389712]
17. Liu X; Xiang JJ; Zhu DC; Jiang LM; Zhou ZX; Tang JB; Liu XR; Huang YZ; Shen YQ Fusogenic reactive oxygen species triggered charge-reversal vector for effective gene delivery. Adv. Mater 2016, 28, (9), 1743–1752. [PubMed: 26663349]
18. Guan XW; Guo ZP; Lin L; Chen J; Tian HY; Chen XS Ultrasensitive pH triggered charge/size dual-rebound gene delivery system. Nano Lett. 2016, 16 (11), 6823–6831. [PubMed: 27643629]
19. Huang D; Yang F; Wang X; Shen H; You Y; Wu DC Facile synthesis and self-assembly behaviour of pH-responsive degradable polyacetal dendrimers. Polym. Chem 2016, 7, (40), 6154–6158.
20. Huang D; Wang YQ; Yang F; Shen H; Weng ZQ; Wu DC Charge-reversible and pH-responsive biodegradable micelles and vesicles from linear-dendritic supramolecular amphiphiles for anticancer drug delivery. Polym. Chem 2017, 8, (43), 6675–6687.
21. Yuan Q; Lee E; Yeudall WA; Yang H Dendrimer-triglycine-EGF nanoparticles for tumor imaging and targeted nucleic acid and drug delivery. Oral Oncol. 2010, 46 (9), 698–704. [PubMed: 20729136]
22. Schneider CA; Rasband WS; Eliceiri KW NIH image to ImageJ: 25 years of image analysis. Nat. Methods 2012, 9 (7), 671–675. [PubMed: 22930834]
23. Thibault M; Nimesh S; Lavertu M; Buschmann MD Intracellular trafficking and decondensation kinetics of chitosan-pDNA polyplexes. Mol. Ther 2010, 18 (10), 1787–1795. [PubMed: 20628361]
24. Won YW; Yoon SM; Lee KM; Kim YH Poly(oligo-D-arginine) with internal disulfide linkages as a cytoplasm-sensitive carrier for siRNA delivery. Mol. Ther 2011, 19 (2), 372–380. [PubMed: 21081902]
25. Tang MX; Redemann CT; Szoka FC In vitro gene delivery by degraded polyamidoamine dendrimers. Bioconjug. Chem 1996, 7, 703–714. [PubMed: 8950489]
26. Shakhbazau A; Isayenka I; Kartel N; Goncharova N; Seviaryn I; Kosmacheva S; Potapnev M; Shcharbin D; Bryszewska M Transfection efficiencies of PAMAM dendrimers correlate inversely with their hydrophobicity. Int. J. Pharm 2010, 383 (1), 228–235. [PubMed: 19770028]
27. Wang H; Shi H-B; Yin S-K Polyamidoamine dendrimers as gene delivery carriers in the inner Ear: how to improve transfection efficiency. Exp. Ther. Med 2011, 2 (5), 777–781. [PubMed: 22977574]

Author Manuscript Author Manuscript Author Manuscript Author Manuscript

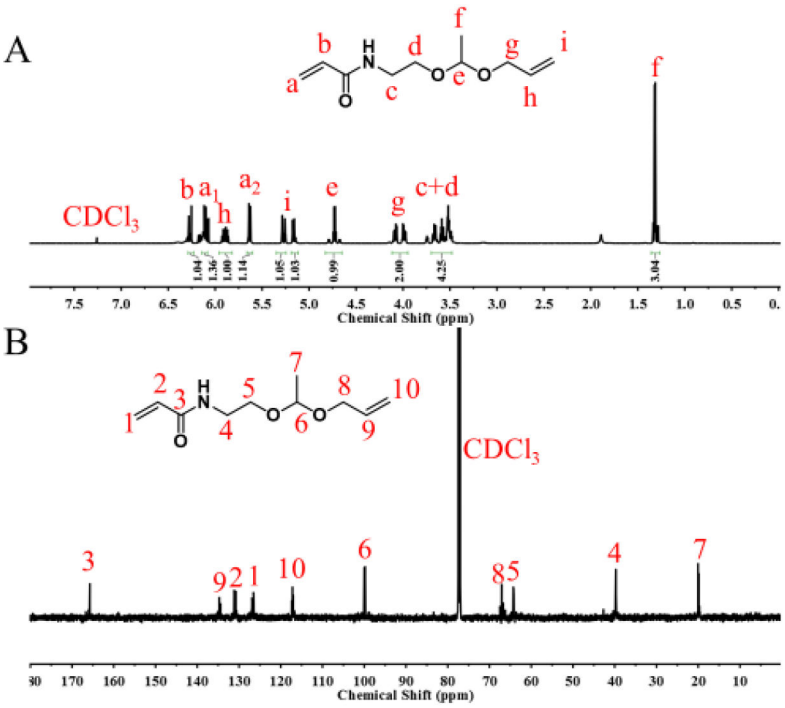

Figure 1.
^{1}H NMR (A) and ^{13}C NMR (B) spectra of AEEAA in $CDCl_3$.

Author Manuscript Author Manuscript Author Manuscript Author Manuscript

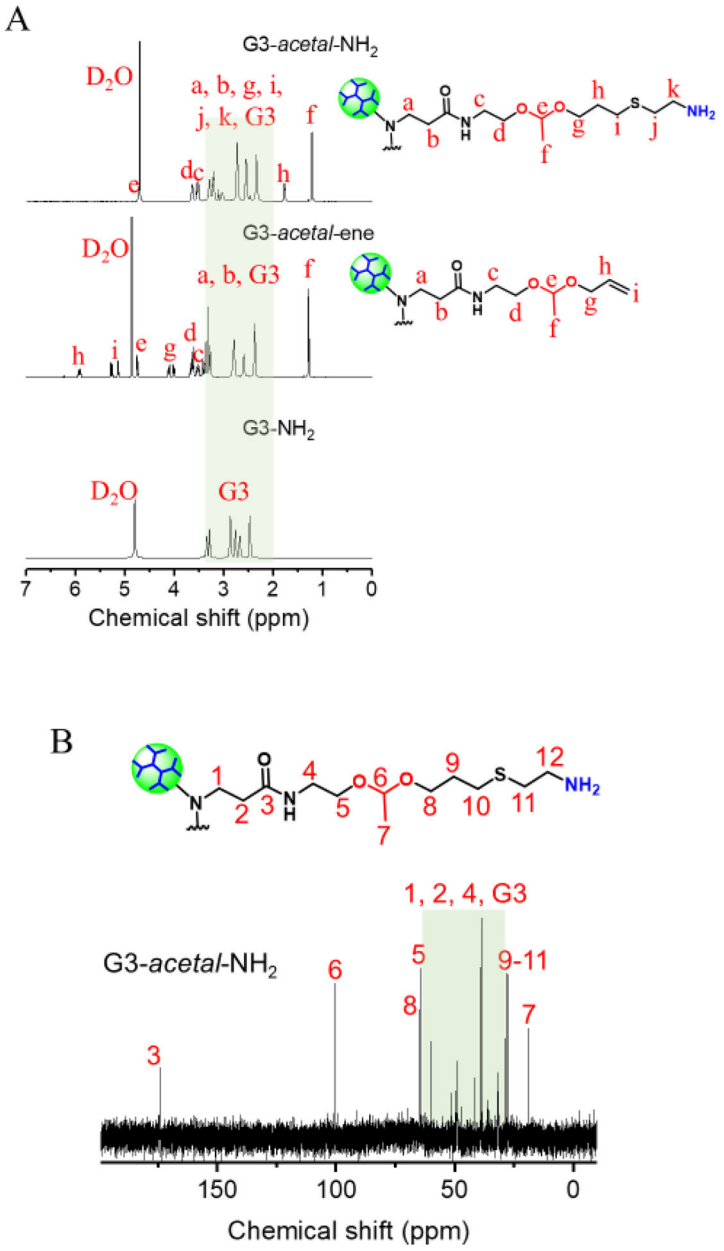

Figure 2.

(A) ^{1}H NMR spectra of G3-*acetal*-NH_2, G3-*acetal*-ene and G3-NH_2 in D_2O. (B) ^{13}C NMR spectrum of G3-*acetal*-NH_2 in D_2O.

Author Manuscript Author Manuscript Author Manuscript Author Manuscript

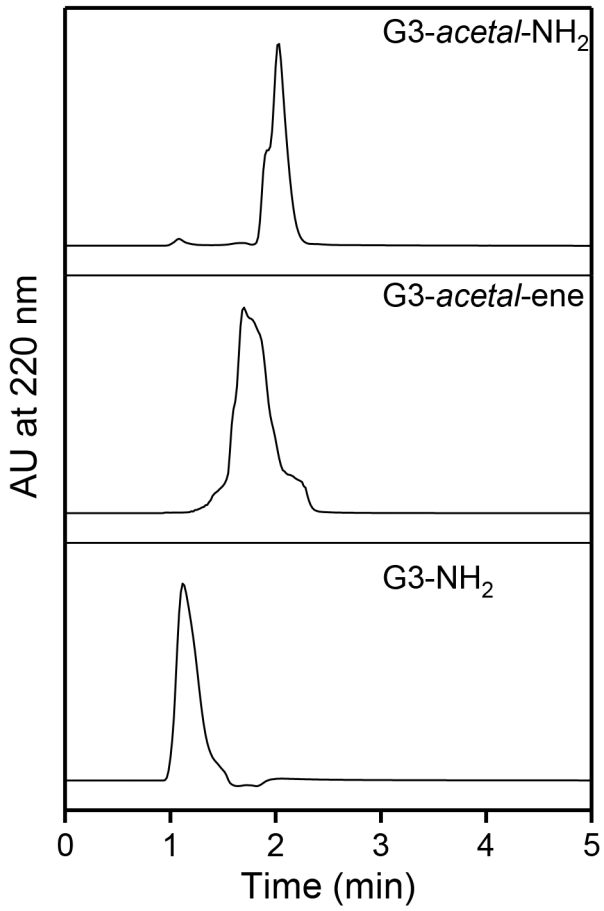

Figure 3.
HPLC analysis of G3-*acetal*-NH_2, G3-*acetal*-ene, and G3-NH_2.

Author Manuscript Author Manuscript Author Manuscript Author Manuscript

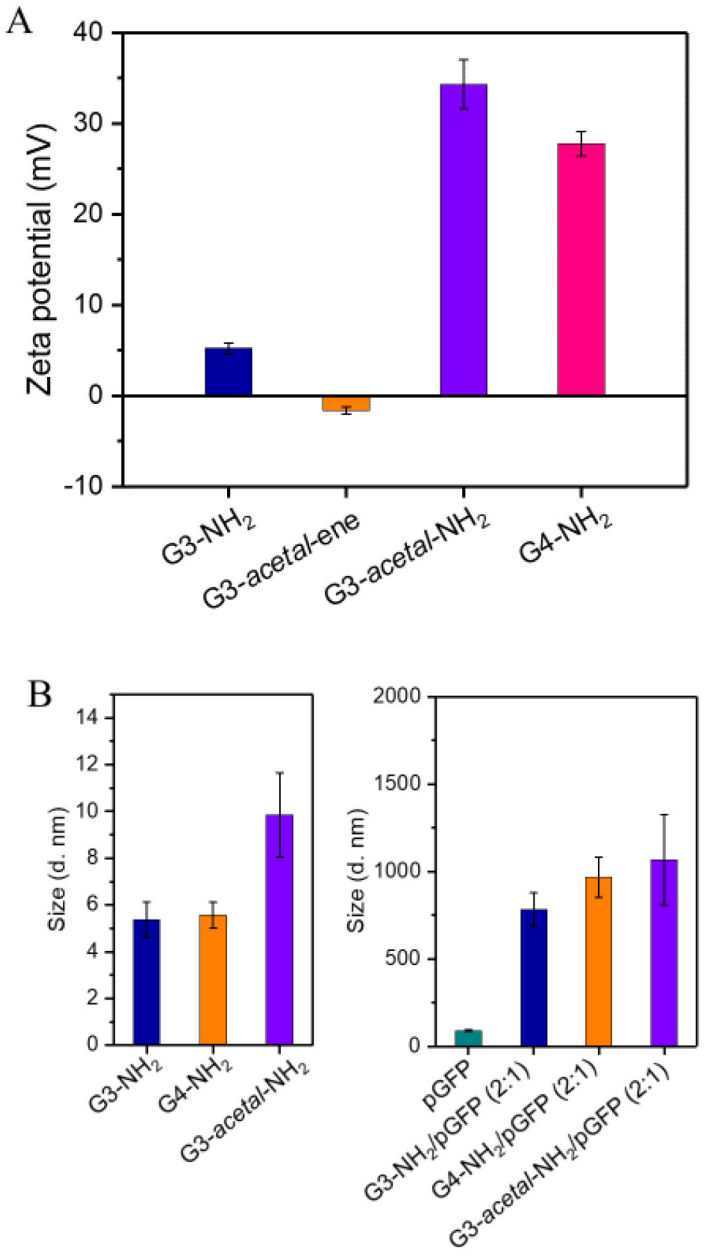

Figure 4.

(A) ζ-potentials of G4-NH_2, G3-*acetal*-NH_2, G3-*acetal*-ene, and G3-NH_2. (B) Hydrodynamic sizes of G3-NH_2, G4-NH_2, G3-*acetal*-NH_2, and their complexes with pGFP.

Author Manuscript Author Manuscript Author Manuscript Author Manuscript

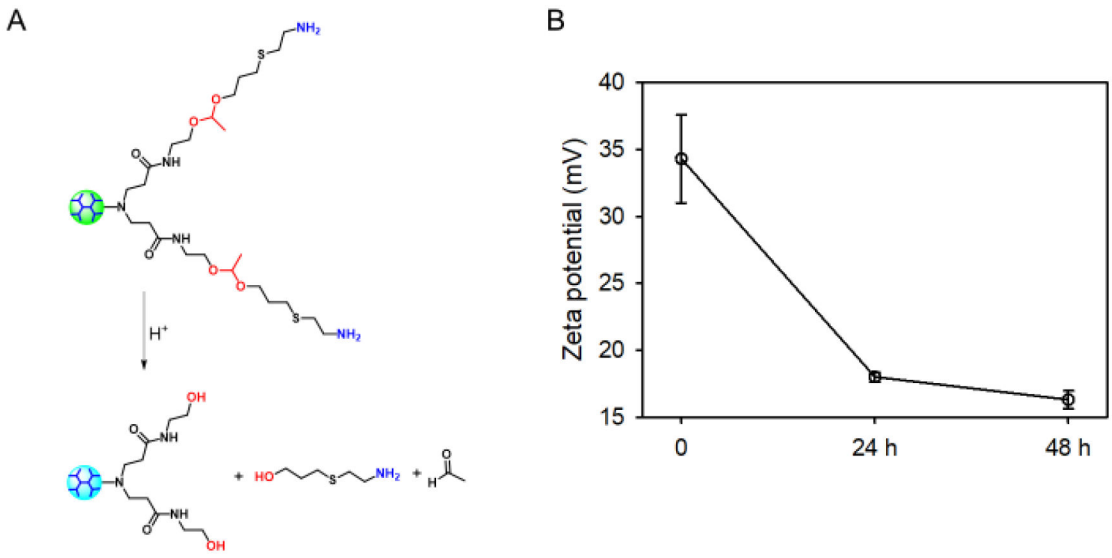

Figure 5.

(A) The acid-responsive charge-reversal of G3-*acetal*-NH_2. (B) ζ-potential change of G3-*acetal*-NH_2 incubated pH=5.3 over the course of incubation at pH=5.3 for 48 h.

Author Manuscript Author Manuscript Author Manuscript Author Manuscript

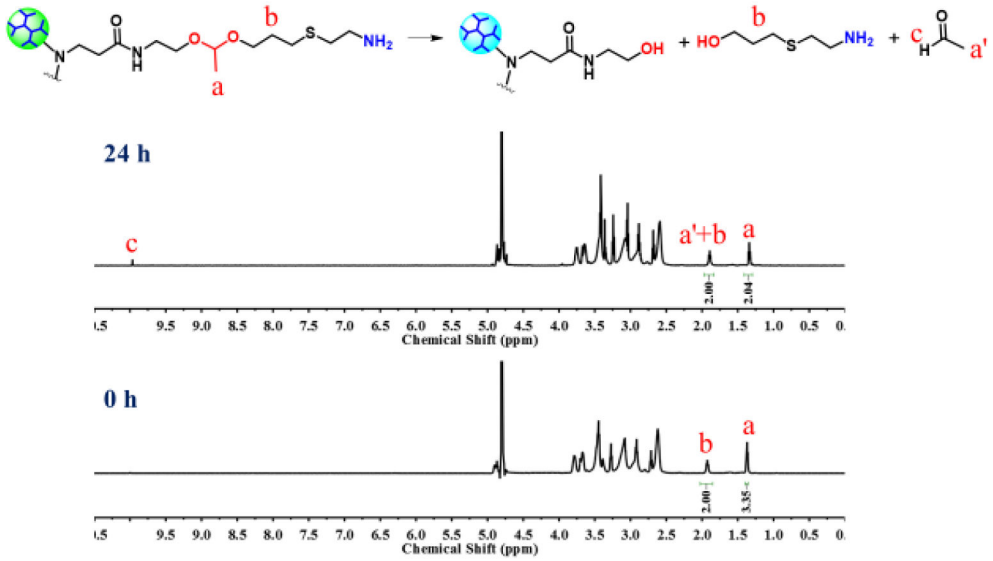

Figure 6.

Monitoring the structural change of G3-*acetal*-NH_2 at pH=5.3 for 24 h in D_2O by using ^1H NMR spectroscopy.

Author Manuscript Author Manuscript Author Manuscript Author Manuscript

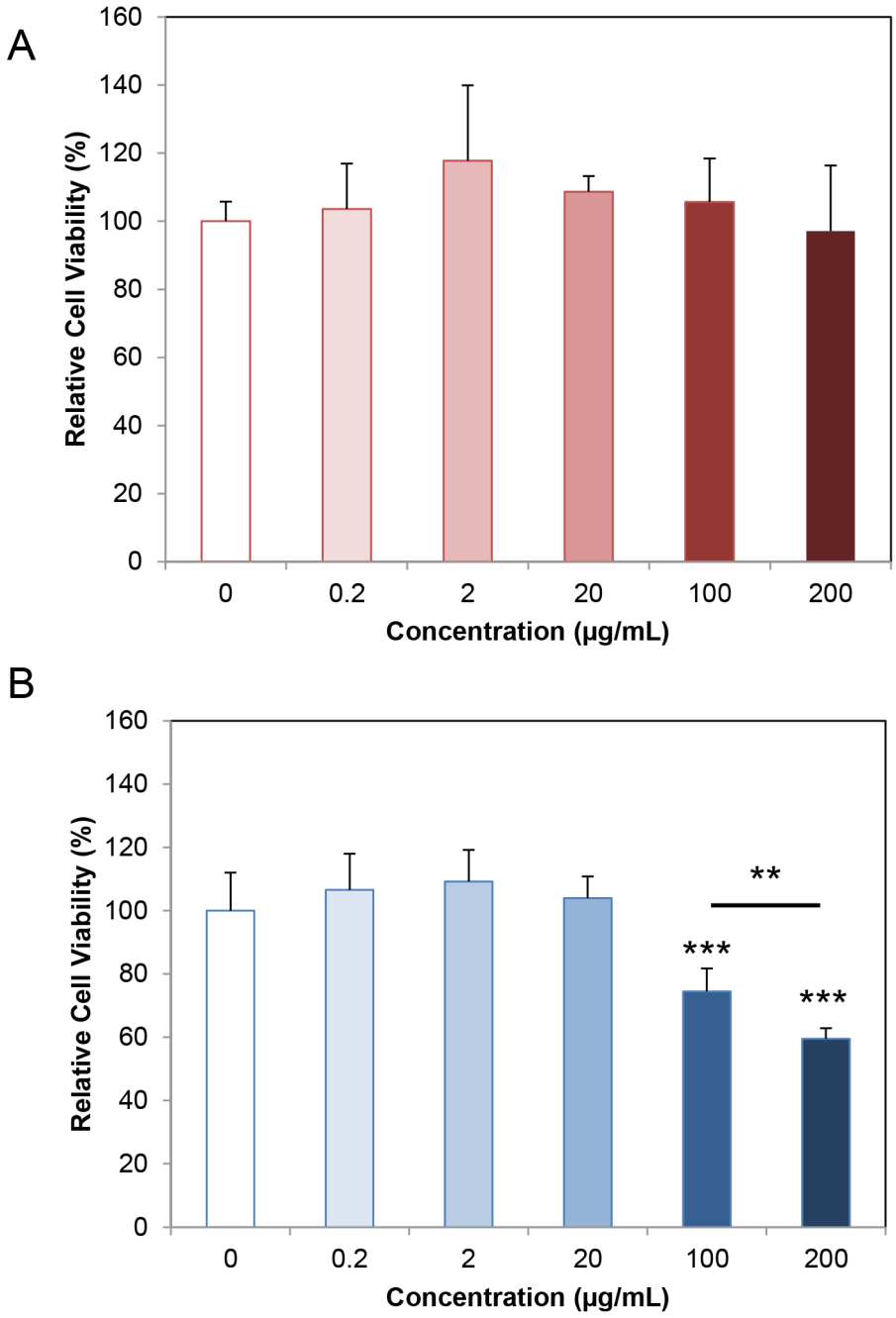

Figure 7.
Cytotoxicity of G3-*acetal*-NH_2 on NIH3T3 cells (A) and HN12 cells (B).

Author Manuscript Author Manuscript Author Manuscript Author Manuscript

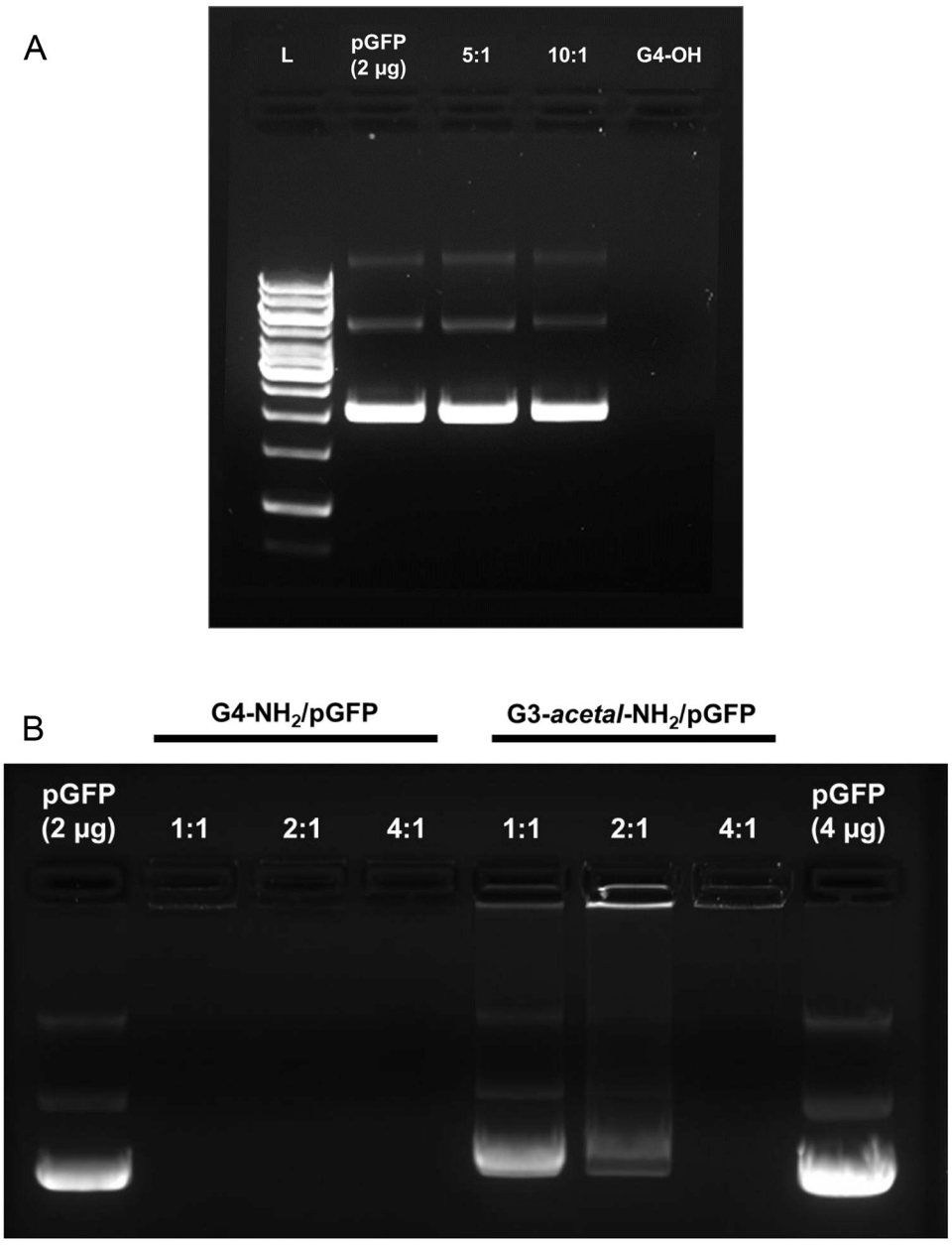

Figure 8.

Gel retardation assay. (A) G4-OH/pGFP complexes at weight ratios of 5 and 10 (L: Ladder, pGFP, 5:1, 10:1, 10:0). (B) G4-NH_2/pGFP and G3-*acetal*-NH_2/pGFP complexes at weight ratios of 1:1, 2:1 and 4:1.

Author Manuscript Author Manuscript Author Manuscript Author Manuscript

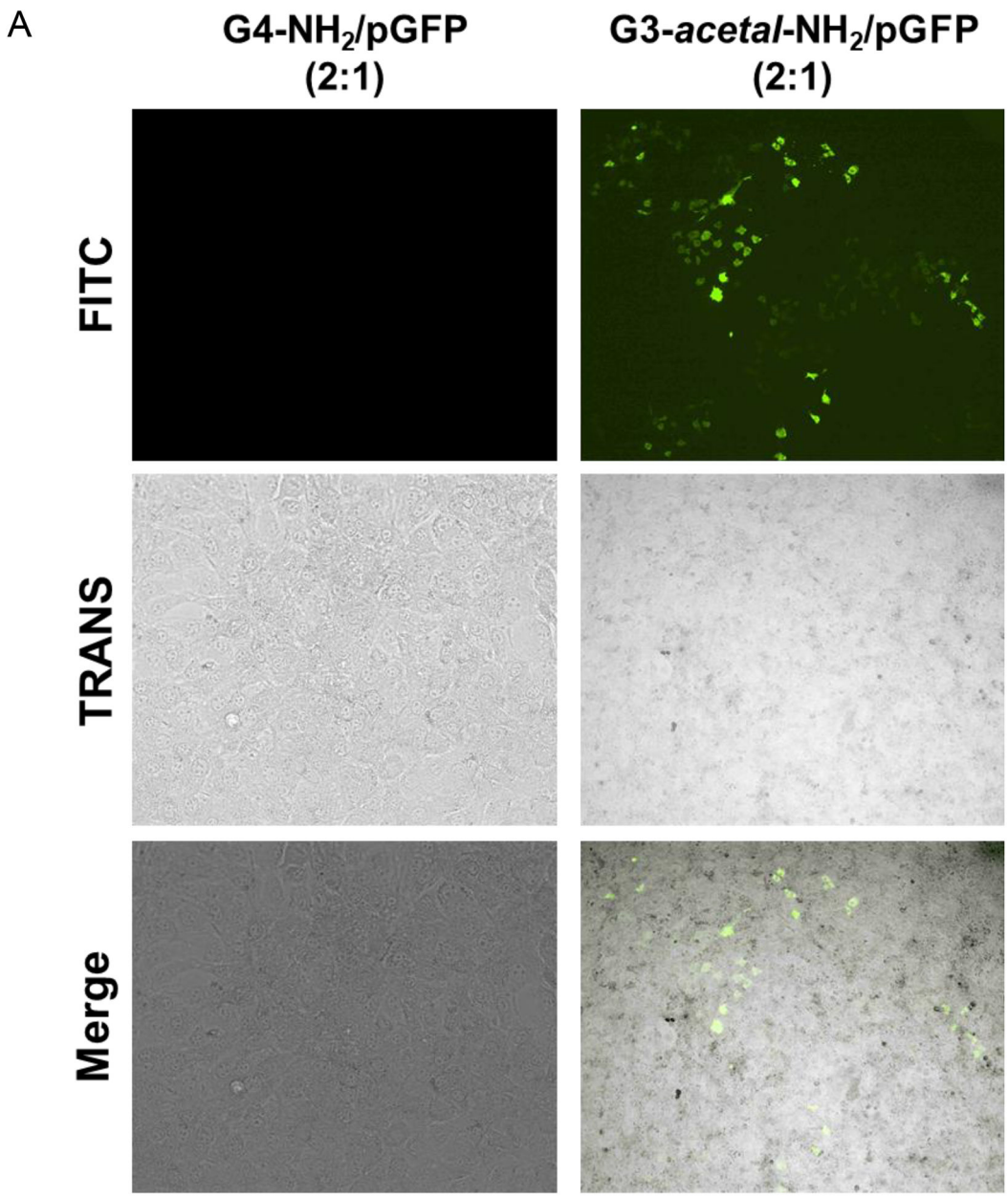

Author Manuscript Author Manuscript Author Manuscript Author Manuscript

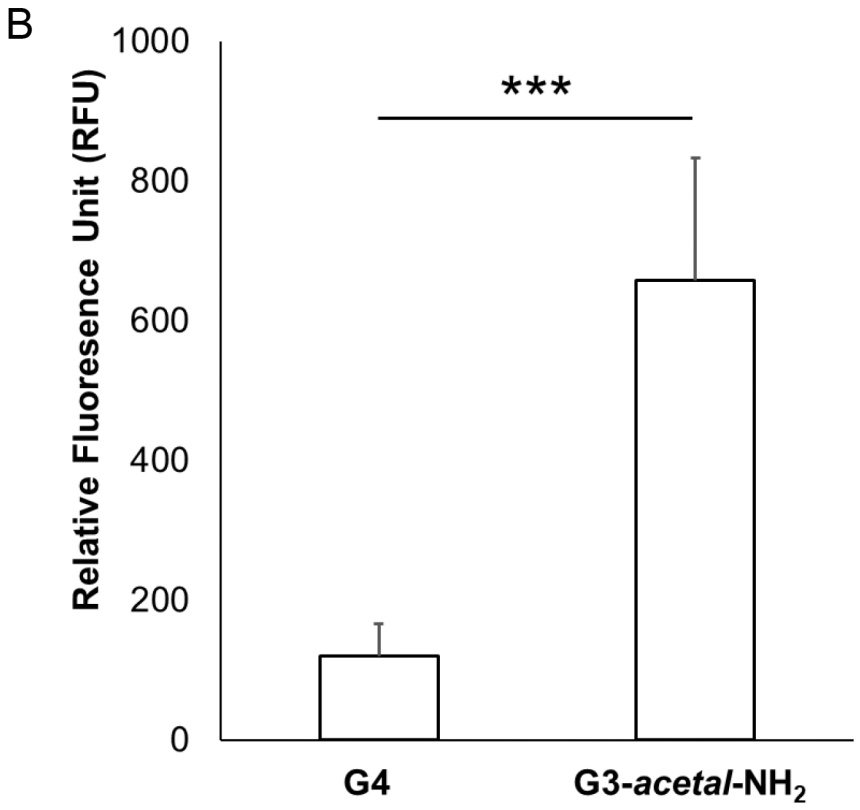

Figure 9.

(A) Fluorescence images (4×) of NIH3T3 cells treated with G4-NH_2/pGFP or G3-*acetal*-NH_2/pGFP. No transfected cells were detected in the G4-NH_2/pGFP group at the 2:1 ratio. (B) Relative fluorescence of extracted protein from cell lysate. The cells treated with G4-NH_2/pGFP and G3-*acetal*-NH_2/pGFP were lysed, and whole protein quantified relative to untreated NIH3T3 cells. Proteins expressing GFP were detected using a NanoDrop3300 fluorospectrometer. ***, $p < 0.001$.

Author Manuscript Author Manuscript Author Manuscript Author Manuscript

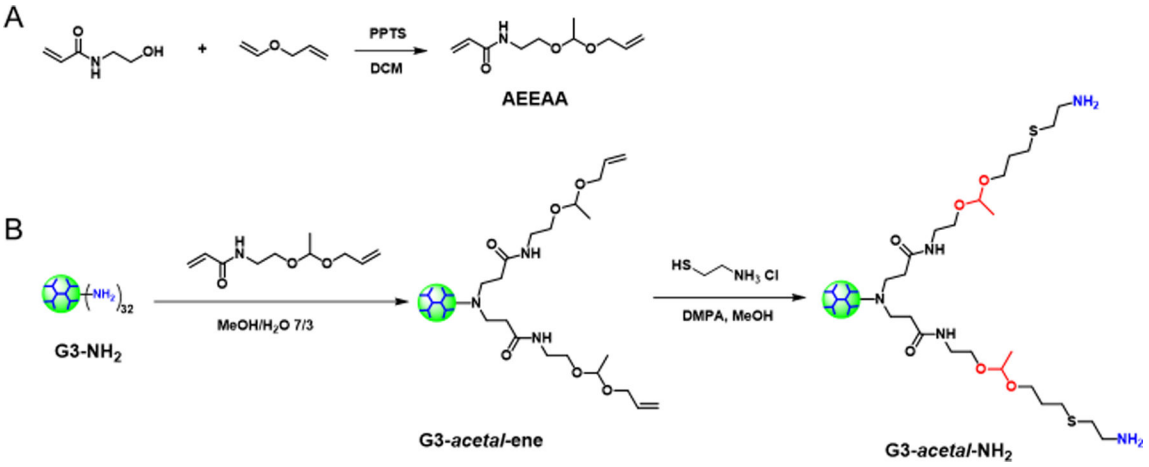

Scheme 1.
Synthetic routes for (A) AEEAA and (B) G3-*acetal*-NH_2.